Pergamon

0301-9322(94)E0029-I

Int. J. Multiphase Flow Vol. 20, No. 5, pp. 819–836, 1994

0301-9322/94 $7.00 + 0.00

TWO-PHASE PRESSURE DROP AND PHASE DISTRIBUTION AT A HORIZONTAL TEE JUNCTION

J. R. BUELL†, H. M. SOLIMAN and G. E. SIMS

Department of Mechanical and Industrial Engineering, University of Manitoba, Winnipeg, Manitoba, Canada R3T 2N2

(Received 7 December 1992; in revised form 1 April 1994)

Abstract—Experimental data are presented for the phase distribution and junction pressure drops of low-pressure (1.5 bar) air–water mixtures at a horizontal, equal-sided (37.6 mm i.d.) dividing tee junction. These data correspond to inlet flow regimes of stratified, wavy, slug and annular flow with inlet superficial liquid velocities $J_{L1} < 0.2$ m/s, for which very limited pressure-drop information is currently available. The phase-distribution data are shown to be in good agreement with data and models available in the literature. Comparisons are made between the present pressure-drop data and existing models, thus identifying the models whose applicability can be extended to the present limiting conditions.

Key Words: pressure drop, phase distribution, dividing tee junction, experimental

1. INTRODUCTION

Branching junctions are common features of the piping networks used for single-phase and two-phase flow distribution systems. These networks are essential components of many facilities in the power and process industries, such as conventional steam power plants, boiling-water and pressurized-water nuclear reactors and a wide variety of chemical and petroleum applications. Knowledge of the pressure drop and phase distribution at a branching junction is important since these parameters can have significant effects on the operation and efficiency of all components downstream from the junction.

The relevance of this problem to many industrial applications, as well as its rather fundamental nature, have motivated significant research in the recent literature, as well as four state-of-the-art reviews by Azzopardi (1986), Lahey (1986), Muller & Reimann (1991) and Azzopardi & Hervieu (1992). Limiting ourselves to tee junctions with horizontal main and branch sides, we find experimental and/or theoretical investigations of this problem reported by Tsuyama & Taga (1959), Collier (1976), Hong (1978), Whalley & Azzopardi (1980), Henry (1981), Saba & Lahey (1984), Seeger *et al.* (1986), Reimann & Seeger (1986), Shoham *et al.* (1987), Ballyk *et al.* (1988), Rubel *et al.* (1988), Hwang *et al.* (1988), Hwang & Lahey (1988), Azzopardi *et al.* (1988), Ballyk & Shoukri (1990) and Hart *et al.* (1991). These research efforts have shown that, in general, the phases are not distributed evenly at the junction and that the pressure drops associated with two-phase flow are significantly higher than those for single-phase flow. While each of the previous investigations has contributed positively to our current state of knowledge, it is fair to note that, due to the complexity of the problem, a full understanding of all relevant phenomena has not been achieved yet (Azzopardi & Hervieu 1992).

The pressure drop and phase distribution at branching junctions are dependent on a large number of variables such as the inlet flow regime, inlet quality x_1, inlet mass flow rate W_1, branch-to-inlet diameter ratio D_3/D_1, fluid properties, junction geometry and the extraction rate W_3/W_1, where W_3 is the branch mass flow rate. Working towards the ultimate goal of establishing generalized predictive models, it is essential to develop a database covering wide ranges of the independent variables so that comparisons and validations can be made. Only a few of the two-phase experiments mentioned above reported elaborate differential pressure measurements

†Present address: AECL Research, Pinawa, Manitoba, Canada R0E 1L0.

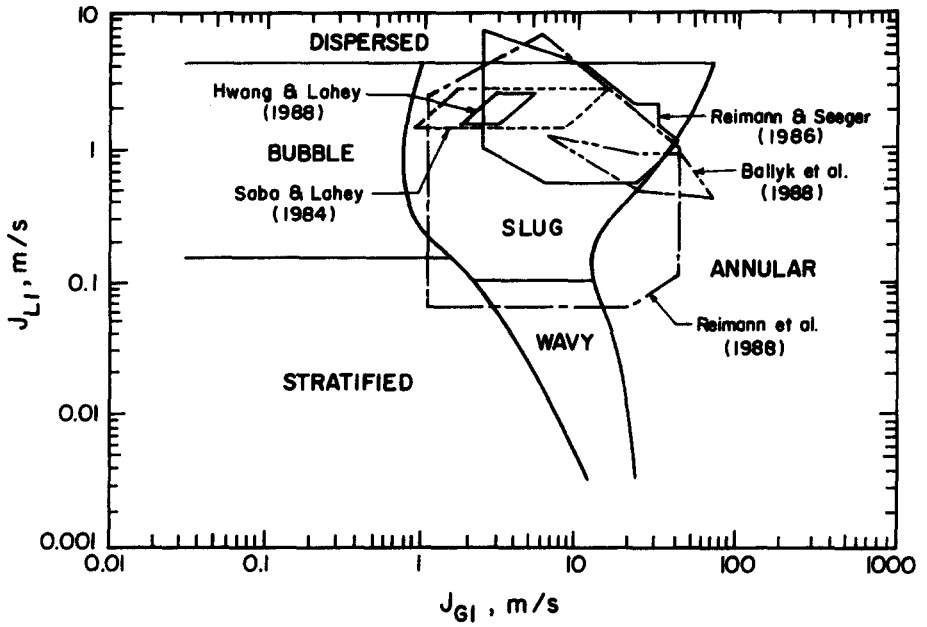

Figure 1. Range of inlet conditions covered in previous pressure-drop experiments plotted on the map of Mandhane *et al.* (1974).

along the inlet, run and branch sides of the junction. Such detailed measurements are necessary in order to properly separate the inlet-to-run and the inlet-to-branch pressure differences, ΔP_{12} and ΔP_{13}, respectively, from the frictional and gravitational pressure differences. In view of the fact that none of the available pressure-drop models is capable of satisfactory predictions for arbitrary flow parameters, with occasionally orders of magnitudes of deviations between data and predictions (Reimann *et al.* 1988), the need for more data becomes obvious. Figure 1 shows the range of inlet conditions for which elaborate measurements of the pressure distribution were made for two-phase flow through horizontal tee junctions. It is clear that the pressure-drop database is deficient for inlet liquid superficial velocities $J_{LI} < 0.1$ m/s.

The objective of the present experimental investigation is to expand the existing database by generating new pressure-drop and phase-distribution data for inlet conditions given by $0.002 < J_{LI} < 0.2$ and $2 < J_{GI} < 40$ m/s. According to figure 1, these conditions should result in stratified, wavy, slug and annular flow regimes in the inlet side of the junction. The geometry under consideration is a horizontal, equal-sided (37.6-mm i.d.) dividing tee junction. Air–water mixtures at inlet conditions of about 1.5 bar and near-ambient temperature are used as the test fluid and extraction rates of $0.1 < W_3/W_1 < 0.9$ are covered. To the authors' best knowledge, the present data of ΔP_{12} and ΔP_{13} are unique; however, the present phase-distribution data overlap partially (in terms of the inlet superficial velocities but not necessarily in terms of junction diameter and fluid properties) with the data of Hong (1978), Shoham *et al.* (1987), Rubel *et al.* (1988), Azzopardi *et al.* (1988) and Hart *et al.* (1991). Where possible, comparisons will be made between the present data and other existing data, models or correlations.

2. EXPERIMENTAL INVESTIGATION

2.1. Flow loop

The flow loop, which was designed and constructed for this investigation, is shown schematically in figure 2. Controlled amounts of distilled water were circulated by a centrifugal pump equipped with a by-pass line. Water flow was mixed in a mixing tee with air supplied from an air compressor. Necessary equipment was installed in the air and water supply lines to allow for pressure and flow-rate regulation, as well as filtering of both streams. A developing length of 67.5 pipe diameters was allowed downstream from the mixer before the two-phase mixture entered the visual section,

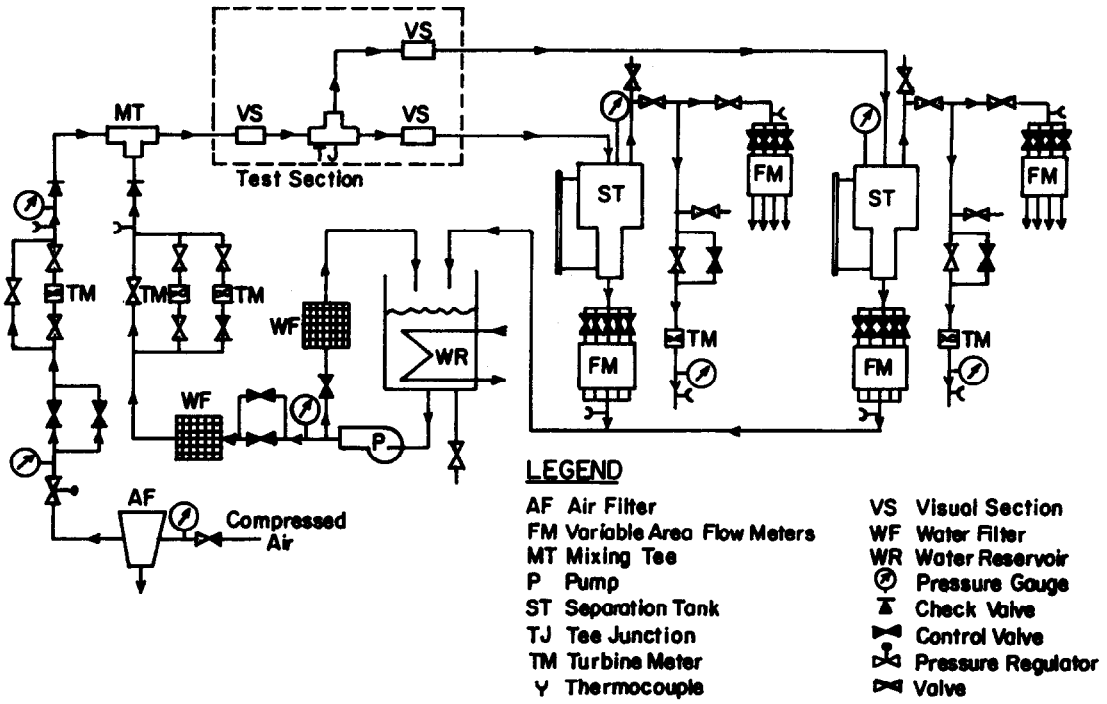

Figure 2. Experimental test facility.

and a further 42 pipe diameters were provided before entering the junction. The two streams emerging from the junction were directed to their respective separation tank, where the individual flows of air and water were separated and then measured downstream from the tank. Water flows from the two separation tanks were rejoined and returned to the water reservoir, while both air flows were discharged to the atmosphere. A throttling valve on the air side downstream from each separation tank was used to control both the extraction rate W_3/W_1 and the inlet pressure to the junction P_1. All piping used for the construction of the test section was commercial type K copper tubing with a 37.6-mm i.d. A surveying level was used to ensure horizontality of the test section (inlet, run and branch sides).

In order to ensure consistency with other research laboratories, a square-edged tee was used. The three sides of the tee were machined to close tolerances in a brass block. This tee is identical to the one used by Rubel *et al.* (1988), who reported the details of the tee construction.

2.2. Instrumentation

The inlet water flow rate W_{L1} was measured using two turbine meters arranged in parallel. These meters had overlapping ranges with maximum capacities of 1.13 and 0.3 m^3/h. The inlet air flow rate W_{G1} was measured using a single turbine meter with a calibrated flow range of 0.11–4.53 m^3/min at standard conditions. The liquid flow rates downstream from the run separation tank W_{L2}, and the branch separation tank W_{L3}, were each measured with a separate bank of five rotameters with overlapping ranges. Each of the two flow-measurement stations was capable of accurate metering over the range 0.0035–13.4 l/min. The run and branch air flow rates, W_{G2} and W_{G3}, respectively, were metered by two separate measuring stations. Each station consisted of a turbine meter for the high flow rates and a bank of four rotameters for the low flow rates with a combined range of 0.056–4530 l/min at standard conditions. All rotameters and turbine meters (air and water) were calibrated and compared with the manufacturer's calibration. Typical deviations between the two calibrations were found to be within $\pm 2\%$ with a maximum of $\pm 5\%$ at the lowest flow rates.

A total of 41 pressure taps were installed along the inlet, run and branch sides of the test section, as shown in figure 3, in order to measure the pressure distribution around the junction. Each pressure tap contained a 1.6-mm hole, which was drilled through the bottom of the tube wall in order to avoid air entrapment in the water-filled pressure lines between the taps and the pressure

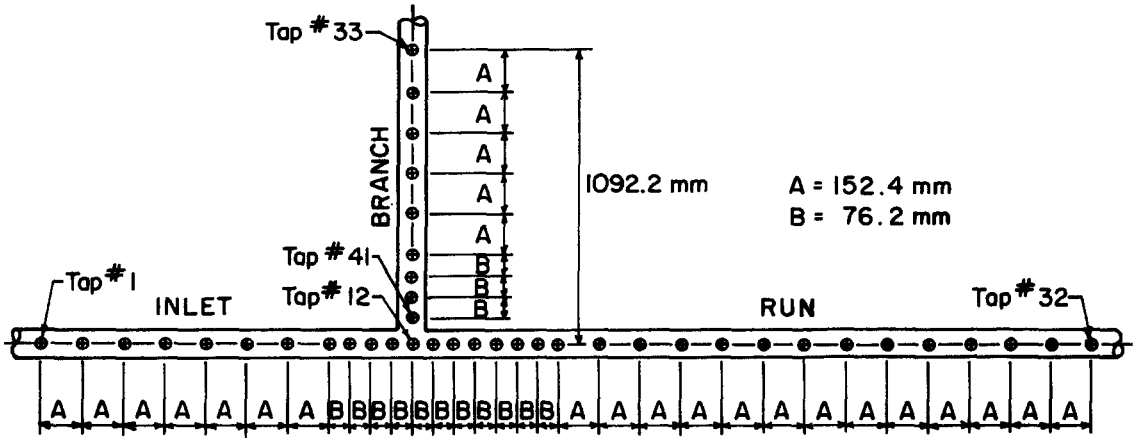

Figure 3. Layout of pressure taps.

transducers. The inlet pressure to the junction P_1 was measured by a pressure transducer connected to pressure tap 11 (see figure 3). The pressure distribution across the 41 taps was determined by a measuring station consisting of two identical banks of differential pressure transducers. Each bank contained three transducers with maximum ranges of approx. ± 45 Pa, ± 550 Pa and ± 5.6 kPa. Using two banks of transducers allowed for immediate cross-checking of results by repeating certain measurements, using two different transducers as described later. All pressure transducers were calibrated using either a micromanometer or a U-tube oil manometer depending on range. In view of the extreme sensitivity of these measurements, the calibration of the transducers was repeated several times during testing to ensure accuracy. As well, the pressure lines between the taps and the transducers were purged before each test to ensure that the lines were free of air.

An elaborate scanning procedure was followed in obtaining the pressure-distribution data. First, taps 13–41 (run and branch) were scanned against tap 1 using the appropriate transducer from one bank, and then the whole scan was repeated using a transducer from the second bank. Next, the pressure in the inlet side (taps 1–12) was scanned against tap 32 in the run using one transducer bank, and then the inlet pressure was scanned again against tap 33 in the branch using the second transducer bank. Thus, two independent sets of data were obtained in each test and the results were accepted only when good agreement was found. Generally, the agreement between transducers from the two banks was maintained within $\pm 2\%$ in all tests. Each single differential pressure measurement was obtained by averaging a transducer output using samples of pressure signals taken over 120 s at the rate of 100 samples per second.

2.3. *Data reduction*

Voltage signals from the turbine meters and the pressure transducers were fed into a data acquisition system. The data acquisition system consisted of an 80286-based microcomputer with two analog-to-digital boards. A computer program was written to control the gathering and reduction of data, thus providing continuous monitoring of the reduced data during the experimental runs.

The inlet, run, and branch mass flow rates W_{L1}, W_{G1}, W_{L2}, W_{G2}, W_{L3} and W_{G3}, were determined using the calibration curve of the appropriate device (turbine meter or rotameter) and the corresponding reading of temperature and/or pressure. These measured flow rates were corrected for evaporation of the liquid phase in the mixer, test section and separation tanks. Details of the procedure followed in these evaporation corrections are described by Buell (1992). For the test runs corresponding to the highest superficial gas velocity $J_{G1} \approx 40$ m/s and the lowest superficial liquid velocity $J_{L1} \approx 0.0023$ m/s, these corrections were found to be significant with up to 20% of the water entering the mixer evaporating before leaving the separation tanks. However, for the vast majority of test runs, which corresponded to lower J_{G1} or higher J_{L1}, these corrections were found to be insignificant. Using the corrected flow rates, it was possible (using the standard definitions) to

calculate the inlet, run and branch mass flow rates, W_1, W_2 and W_3, respectively, the inlet, run and branch qualities, x_1, x_2 and x_3, respectively, the inlet superficial velocities, J_{L1} and J_{G1}, and the fractions of gas and liquid entering the branch, F_{BG} and F_{BL}, respectively.

Mass balance errors were calculated for both phases as the percentage deviation between the inlet flow rate and the sum of the two outlet flow rates from both separation tanks, corrected for evaporation. For air, the mass balance was maintained within $\pm 9\%$ in all test runs, and within $\pm 5\%$ for 82% of the test runs. For water, the mass balance was always within $\pm 7\%$, and for 97% of the test runs, the balance was within $\pm 5\%$.

The junction pressure drops ΔP_{12} and ΔP_{13} were determined from the measured pressure distribution; a sample of which is shown in figure 4 with $(P - P_r)$ as ordinate, where P is the local pressure and P_r is a reference pressure (the pressure at tap 1 in the case shown in figure 4). A significant amount of data showing detailed measurement of the pressure distribution around the junction can be found in Buell (1992). The fully-developed pressure gradients in the inlet, run and branch were extrapolated to the centre of the junction, thus giving the values of P_1, P_2 and P_3, respectively, as shown in figure 4. Obviously, the accuracy of ΔP_{12} and ΔP_{13} is strongly dependent on the estimates of P_1, P_2 and P_3. Therefore, it was extremely important that these extrapolated values were obtained from data which were fully developed. Taking the branch, for example, the pressure readings from the last four pressure taps (farthest away from the junction) were fitted by a linear regression equation that determined the intercept P_3 and the estimated uncertainty in this value (δP_3) using the procedure proposed by Kline & McClintock (1953) and Walpole & Myers (1985). The linear regression was repeated using an increasing number of pressure tap readings, resulting in different values of P_3 and δP_3. In general, the uncertainty δP_3 decreased as the number of points increased up to a maximum number of points beyond which δP_3 increased, which signalled the departure from the fully-developed region. The value of P_3 corresponding to the minimum δP_3 was chosen as the correct intercept, and a similar procedure was followed in the inlet and run sides. This procedure was programmed and used for calculating the present values of ΔP_{12} and ΔP_{13}.

Earlier investigations have shown that the inlet flow regime is an important parameter in determining the phase distribution at junctions. In the present investigation, four major (stratified, wavy, slug and annular) and two transitional (semiannular and stratified-wavy) flow regimes were visually observed. The standard descriptions (e.g. Mandhane *et al.* 1974) were used in identifying the major flow regimes. The following descriptions were used in identifying the transitional regimes:

Semiannular flow. The flow is similar in appearance to annular flow, except that the stable film does not cover the entire tube periphery. The liquid film thickness increases to a maximum at the bottom of the tube, while the top of the tube appears dry.

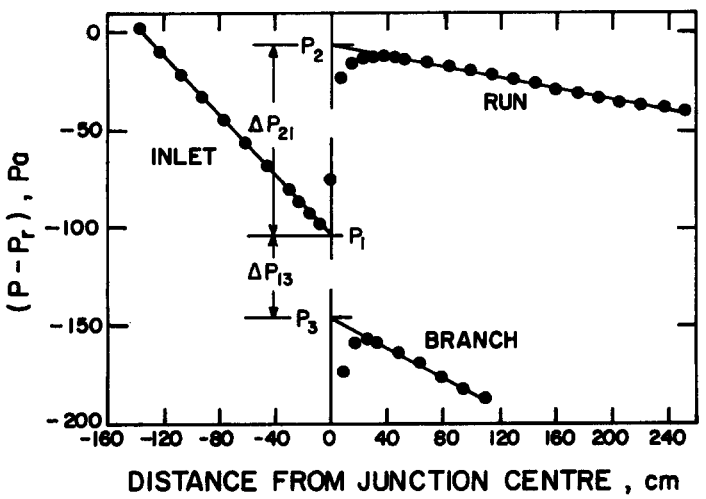

Figure 4. An example of the measured pressure distribution.

Stratified-wavy flow. The gas–liquid interface is mainly smooth in appearance; however, small surface waves appear intermittently.

2.4. Experimental uncertainty

An error analysis was undertaken for all the phase-distribution and pressure-drop data. The procedure followed is according to the method of Kline & McClintock (1953). In the following summary, the uncertainty interval of each variable is based on a 95% confidence level, or odds of approx. 20 to 1. Details are given by Buell (1992).

The experimental uncertainty in the values of J_{GI}, J_{LI} and x_1 was found to be within $\pm 5\%$. For W_3/W_1, x_3/x_1 and F_{BG}, the uncertainty was within approx. $\pm 15\%$, although typical values were near $\pm 6\%$. The uncertainty in F_{BL} ranged between ± 4 and $\pm 25\%$, although values were typically closer to $\pm 10\%$. The errors in the pressure and temperature at the junction inlet were within $\pm 1.3\%$ and ± 0.3°C, respectively.

For the ΔP_{12} data, 94% of the data had uncertainties within $\pm 17\%$. As well, 76% of the ΔP_{13} data had uncertainties within $\pm 30\%$; these figures exclude three data points where ΔP_{13} had an absolute value less than or equal to 1 Pa (at these extremely small pressure drops, the relative error would be expected to be very large).

3. RESULTS AND DISCUSSION

The pressure-drop and phase-distribution data developed in this experimental investigation consist of 15 test groups; all correspond to nominal conditions of 1.5 bar and 21.3°C at the junction inlet. Within each test group, J_{GI}, J_{LI} and the inlet flow regime remained fixed, while W_3/W_1 was varied from 0.1 to 0.9; thus, a total of 76 test runs were performed. The reduced experimental results for all test runs are listed in table 1. As well, the operating conditions of the fifteen test groups

Table 1. Pressure-drop and phase-distribution data

Test No.	J_{GI} (m/s)	J_{LI} (m/s)	P_1 (bar)	T_1 (°C)	x_1 (%)	W_3/W_1	x_3/x_1	ΔP_{21} (Pa)	ΔP_{13} (Pa)	Inlet flow regime
1-1	10.8	0.0398	1.51	22.5	32.5	0.104	1.39	52	−30	
1-2	11.0	0.0398	1.49	21.7	32.6	0.300	1.46	136	4	
1-3	10.9	0.0397	1.50	21.8	32.5	0.513	1.42	156	76	Wavy
1-4	10.8	0.0397	1.50	21.9	32.5	0.716	1.30	146	133	
1-5	10.8	0.0401	1.51	22.1	32.3	0.735	1.30	144	138	
1-6	10.1	0.0399	1.51	21.6	31.0	0.897	1.08	152	153	
2-1	10.9	0.0093	1.52	21.4	67.6	0.108	1.15	39	−23	
2-2	10.9	0.0092	1.51	21.8	67.8	0.309	0.96	73	−14	
2-3	10.9	0.0092	1.51	21.1	67.8	0.499	0.98	99	7	Wavy
2-4	10.9	0.0092	1.51	20.3	67.9	0.706	0.96	98	43	
2-5	11.0	0.0092	1.49	19.6	68.0	0.906	0.94	96	96	
3-1	2.7	0.0399	1.50	21.2	10.6	0.100	0.00		0	
3-2	2.7	0.0400	1.51	21.2	10.7	0.299	0.56		5	
3-3	2.7	0.0398	1.49	21.2	10.7	0.502	1.11		7	Wavy
3-4	2.7	0.0398	1.50	21.1	10.6	0.692	1.39		22	
3-5	2.7	0.0397	1.49	21.2	10.7	0.898	1.10	9	20	
4-1	10.9	0.1796	1.49	21.2	9.7	0.102	1.63	85	−45	
4-2	10.9	0.1801	1.49	21.2	9.6	0.307	2.67		181	
4-3	11.0	0.1793	1.51	21.0	9.8	0.490	1.92	272	347	Slug
4-4	10.8	0.1802	1.50	21.2	9.6	0.699	1.35		519	
4-5	10.4	0.1797	1.48	21.0	9.2	0.898	1.05	337	514	
5-1	4.4	0.1800	1.50	20.9	4.2	0.105	2.40	33	−37	
5-2	4.4	0.1807	1.52	21.0	4.2	0.311	2.94	207	64	
5-3	4.5	0.1796	1.48	21.3	4.2	0.500	1.84	182	115	Slug
5-4	4.1	0.1797	1.49	21.5	3.8	0.693	1.37	234	140	
5-5	4.0	0.1798	1.51	21.0	3.8	0.902	1.07	230	218	
6-1	2.7	0.1803	1.51	20.9	2.6	0.099	0.86			
6-2	2.7	0.1793	1.54	21.0	2.6	0.301	2.77			
6-3	2.7	0.1806	1.50	20.9	2.6	0.510	1.77	183	93	Slug
6-4	2.7	0.1801	1.50	20.9	2.6	0.703	1.38	182	150	
6-5	2.7	0.1801	1.51	21.0	2.6	0.899	1.10	185	167	

continued

Table 1—*continued*

7-1	10.9	0.0022	1.51	20.0	89.8	0.096	1.00	24	−16	
7-2	10.8	0.0022	1.51	20.0	89.8	0.298	0.85	50	−17	
7-3	10.1	0.0021	1.49	16.6	89.6	0.504	0.87		1	Stratified-wavy
7-4	11.0	0.0022	1.51	20.0	89.8	0.684	0.94		32	
7-5	11.2	0.0022	1.49	19.6	89.8	0.884	0.98		89	
8-1	4.4	0.0094	1.50	19.2	45.5	0.098	1.26			
8-2	4.4	0.0095	1.51	18.8	45.3	0.297	1.10			
8-3	4.5	0.0094	1.48	21.4	45.4	0.505	1.01			Stratified-wavy
8-4	4.4	0.0094	1.51	22.6	45.4	0.694	1.01			
8-5	4.5	0.0094	1.49	22.4	45.2	0.883	0.99			
9-1	2.7	0.0023	1.51	22.0	67.4	0.094	0.96			
9-2	2.7	0.0023	1.50	23.2	67.9	0.278	0.95			
9-3	2.7	0.0022	1.51	21.7	68.1	0.451	0.90			Stratified
9-4	2.7	0.0023	1.51	21.6	67.5	0.538	0.89			
9-5	2.7	0.0023	1.52	22.0	67.4	0.658	0.89			
9-6	2.7	0.0023	1.49	21.7	67.5	0.847	0.93			
10-1	2.7	0.0094	1.51	23.8	33.3	0.100	0.60			
10-2	2.7	0.0094	1.50	22.4	33.5	0.284	1.03			
10-3	2.7	0.0094	1.50	22.0	33.5	0.491	1.07			Stratified
10-4	2.7	0.0094	1.50	21.8	33.5	0.685	0.94			
10-5	2.7	0.0095	1.50	21.5	33.4	0.857	1.08			
11-1	18.3	0.0098	1.50	22.2	76.6	0.104	0.88	68	−33	
11-2	18.3	0.0098	1.51	22.4	76.7	0.300	0.94	180	−41	
11-3	18.2	0.0098	1.49	21.3	76.6	0.501	0.96	232	29	Semiannular
11-4	18.4	0.0098	1.49	22.6	76.8	0.699	0.99	267	133	
11-5	18.4	0.0098	1.49	22.2	76.7	0.894	0.97	251	269	
12-1	40.9	0.0018	1.49	23.2	97.5	0.101	0.89	343	−120	
12-2	40.5	0.0019	1.50	22.1	97.4	0.298	0.94	705	−148	
12-3	40.3	0.0017	1.51	24.6	97.6	0.498	0.97	981	86	
12-4	40.4	0.0018	1.50	22.6	97.5	0.699	0.99	1172	591	Annular
12-5	40.9	0.0018	1.49	21.6	97.6	0.899	1.00	993	1444	
13-1	40.5	0.0096	1.51	23.5	88.2	0.100	0.71	324	−99	
13-2	39.2	0.0096	1.58	22.4	88.4	0.301	0.89	860	−120	
13-3	40.8	0.0096	1.50	21.5	88.3	0.499	0.90	1132	121	Annular
13-4	41.1	0.0096	1.49	21.8	88.3	0.701	0.95	1212	725	
13-5	40.8	0.0095	1.50	22.3	88.3	0.895	0.99	1064	1574	
14-1	40.3	0.0394	1.51	16.3	64.9	0.098	0.49	318	−104	
14-2	40.7	0.0394	1.49	17.5	64.7	0.297	0.93	1019	0	
14-3	40.6	0.0396	1.49	21.2	64.3	0.495	1.05	1421	451	Annular
14-4	40.2	0.0395	1.50	21.3	64.2	0.702	1.07	1474	1251	
14-5	40.3	0.0396	1.54	22.6	64.8	0.900	1.09	1366	2412	
15-1	38.1	0.1791	1.80	22.5	31.1	0.101	0.93	688	−79	
15-2	40.2	0.1797	1.50	17.2	28.7	0.299	1.67	2666	715	
15-3	39.8	0.1795	1.55	22.0	28.8	0.506	1.70	2619	2574	Annular
15-4	33.9	0.1792	1.78	22.0	28.4	0.700	1.43	2162		

are shown in figure 5 plotted on the flow regime map of Mandhane *et al.* (1974). Good agreement can be seen between the present observations and the predictions of the map. It is also interesting to note that the present data cover a fairly wide area on the map with a factor of about 100 in J_{Ll} and over 10 in J_{Gl}. In terms of inlet mass flux and quality, the present data cover the range $7 < G_l < 259$ kg/m^2 s and $0.026 < x_l < 0.976$.

3.1. Phase-distribution data

The major independent variables in the present experiment are J_{Gl} and J_{Ll}, as illustrated in figure 5. The influence of each of these variables on the phase distribution was studied separately. Comparisons in terms of magnitude and trend were also made with other experimental data and analytical models or empirical correlations.

Figure 6 is representative of the influence of J_{Ll} on the phase-distribution phenomenon. This data segment corresponds to annular flow with $J_{Gl} = 40$ m/s and various values of J_{Ll}. The value of F_{BL} slightly exceeds one at a few data points in this figure and other succeeding figures; this is due to the unavoidable mass balance error discussed earlier. Based on our visual observations showing no liquid flow in the run during these tests, F_{BL} can be practically taken as one at these points.

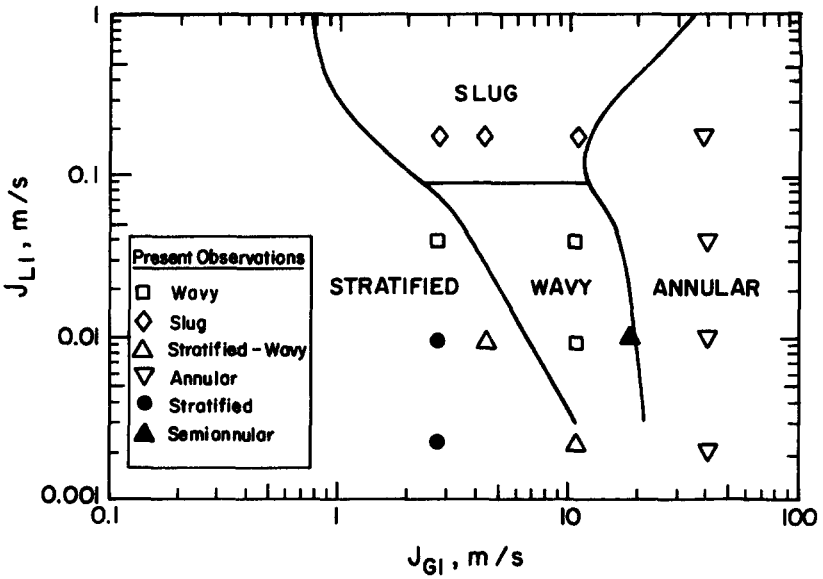

Figure 5. Range of inlet conditions covered in present experiment.

Figure 6 shows clearly that for a fixed J_{GI}, the preference of the gas to exist through the branch increases as J_{LI} increases. These data also demonstrate the complexity of the phase-distribution phenomenon, where the trend changes from strong preference for the liquid to enter the branch to strong preference for the gas to enter the branch as the phase velocities vary within the same flow regime.

The trend in figure 6 was found to apply generally to all the present data and it is consistent with the trends observed by Hong (1978), Shoham *et al.* (1987) and Rubel *et al.* (1988). This trend can be explained using the ideas suggested by Hwang *et al.* (1988) and Azzopardi *et al.* (1988), whereby an increase in J_{LI} results in an increase in the average axial momentum of the liquid phase and consequently, a decrease in the probability of the liquid to enter the branch.

Studying the effect of varying J_{GI} at a fixed J_{LI} failed to produce consistent trends. For example, at the highest liquid velocity $J_{LI} = 0.18$ m/s, the effect of J_{GI} was found to be very small. At the lowest liquid velocity $J_{LI} = 0.0021$ m/s, increasing J_{GI} increased the liquid preference to enter the branch, while at $J_{LI} = 0.04$ m/s, increasing J_{GI} first increased the gas preference to enter the branch

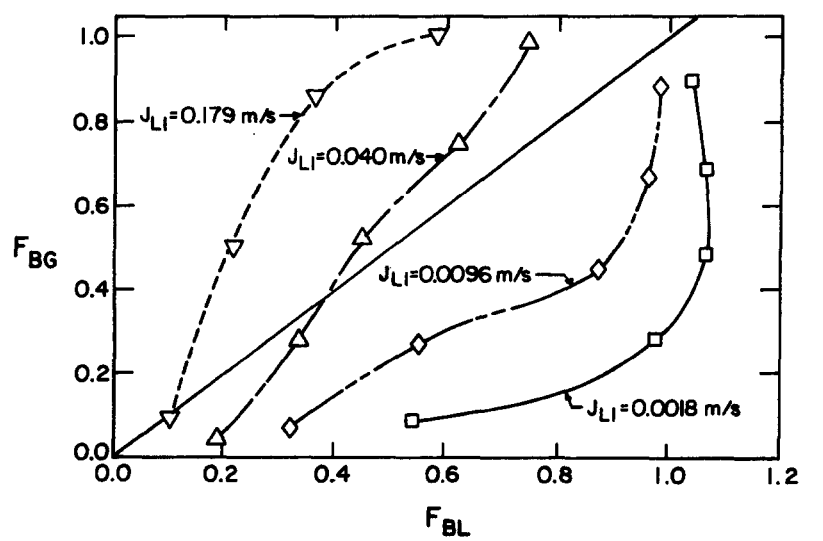

Figure 6. Effect of J_{LI} on the phase distribution for annular flow with $J_{GI} = 40$ m/s.

and then the trend reversed. Some of these trends can be explained with the principle of relative momentum discussed above; however, the picture here is complicated due to the flow regime transitions encountered with changing J_{GI}. More discussion of the J_{GI}-influence is reported by Buell (1992).

In general (with only one exception), the present data were found to be in good quantitative agreement with other data when the operating conditions were reasonably similar. An example of such good agreement is shown in figure 7 using the present data for $J_{GI} = 10.8$ m/s and the data of Azzopardi *et al.* (1988) for $J_{GI} = 12$ m/s. The data of Azzopardi *et al.* used in figure 7 correspond to air–water flow at 1.5 bar in an equal sided (38-mm i.d.) horizontal tee junction. Both data show an increasing preference for the gas to enter the branch as J_{LI} increases. As well, the test groups that correspond to close values of J_{LI} are in fairly good quantitative agreement. Other similar comparisons were made by Buell (1992) between segments of the present data and the appropriate segments from the data of Hong *et al.* (1978), Shoham *et al.* (1987), and Rubel *et al.* (1988) showing reasonably good quantitative agreements at close values of J_{LI} and J_{GI}.

The one serious disagreement is illustrated in figure 8 in which data from Shoham *et al.* (1987) at $J_{GI} = 2.5$ m/s, data from Azzopardi *et al.* (1988) at $J_{GI} = 3.0$ m/s and the present data for $J_{GI} = 2.7$ m/s are presented. All data correspond to a stratified flow regime at the junction inlet; however, these segments from Shoham *et al.* and Azzopardi *et al.* correspond to an inlet pressure of 3.0 bar. The data of Shoham *et al.* exhibit strong preference for the gas to exit through the branch, which is in obvious contrast with the present data and those of Azzopardi *et al.* Considering the present test group at $J_{LI} = 0.040$ m/s and the group from Azzopardi *et al.* at $J_{LI} = 0.055$ m/s, we find that the deviation between the two groups at high extraction rates is consistent in trend with the prediction of the relative momentum principle, whereby the lower pressure in the present experiment results in lower gas density, lower gas momentum and consequently higher probability for gas extraction.

Comparisons were also made between the present data and available models and correlations; these results are shown in figures 9–12. Results from the geometrically-based model for annular flow by Azzopardi & Whalley (1982) using the correlation of Kataoka & Ishii (1983) for the entrainment rate are shown in figure 9. Data of annular and semiannular flow are used in this

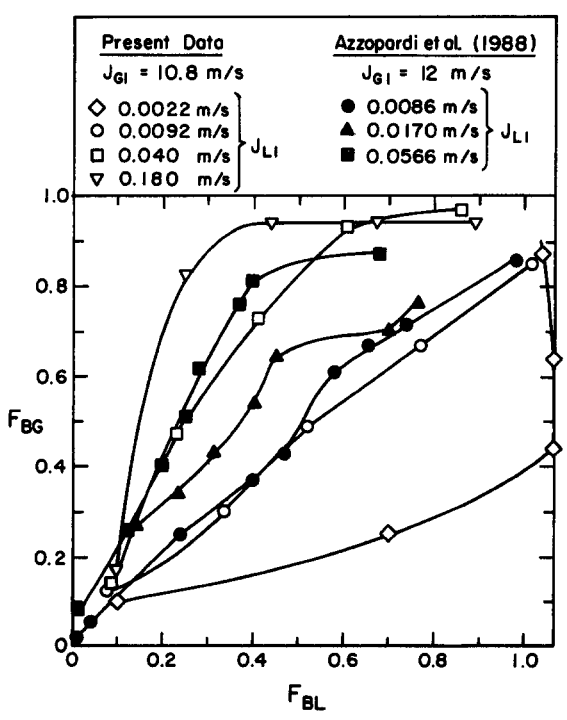

Figure 7. Comparison with other data for $J_{GI} = 10.8$ m/s.

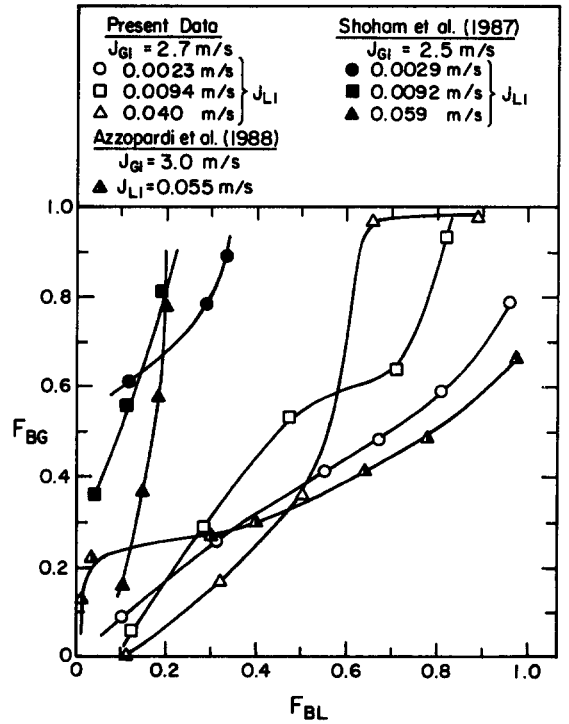

Figure 8. Comparison with other data for $J_{GI} = 2.7$ m/s.

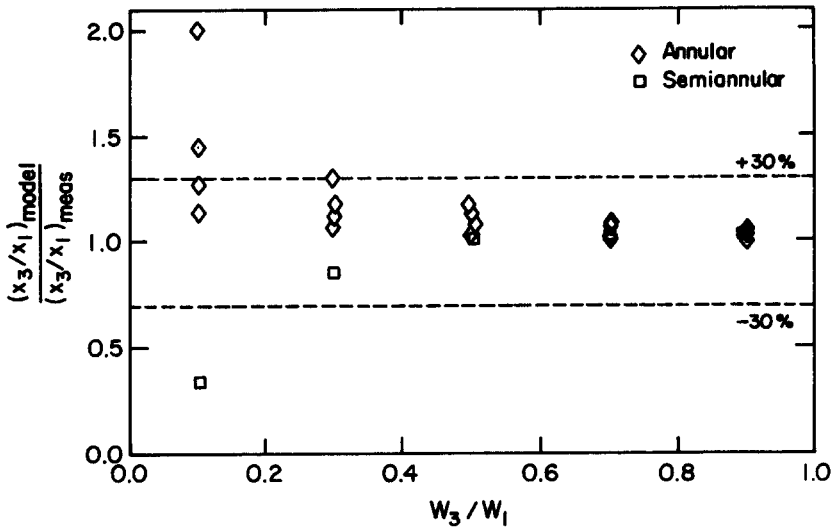

Figure 9. Comparison between the present data of annular and semiannular flow and the model of Azzopardi & Whalley (1982).

comparison. The model's prediction is quite good with 83% of the data predicted within ±30%, and 79% of the data predicted within ±20%. The prediction of the model becomes more precise as the extraction rate increases. A comparison between the empirical correlation of Seeger *et al.* (1986) and all present data is shown in figure 10. Overall, 67% of the data were predicted within ±30% with most of the poor predictions concentrated at low extraction rates. For $W_3/W_1 > 0.3$, the model of Seeger *et al.* produced fairly accurate predictions. Finally the comparison with the model of Hwang *et al.* (1988) is shown in figure 11 for the stratified, stratified-wavy, wavy and slug data and in figure 12 for the annular and semiannular data. In figure 11, 80% of the data are predicted within ±30%. The model does not provide a special treatment for slug flow and these data were entered in the model as wavy flow. Only 47% of the slug data are predicted within ±30%. Excluding slug flow, the model of Hwang *et al.* predicted 94% of the stratified, stratified-wavy, and wavy data within ±30%. Figure 12 shows good performance by this model against the annular and semiannular data as well with 88% of this segment predicted within ±30%. Complete details about the execution of these comparisons are given by Buell (1992).

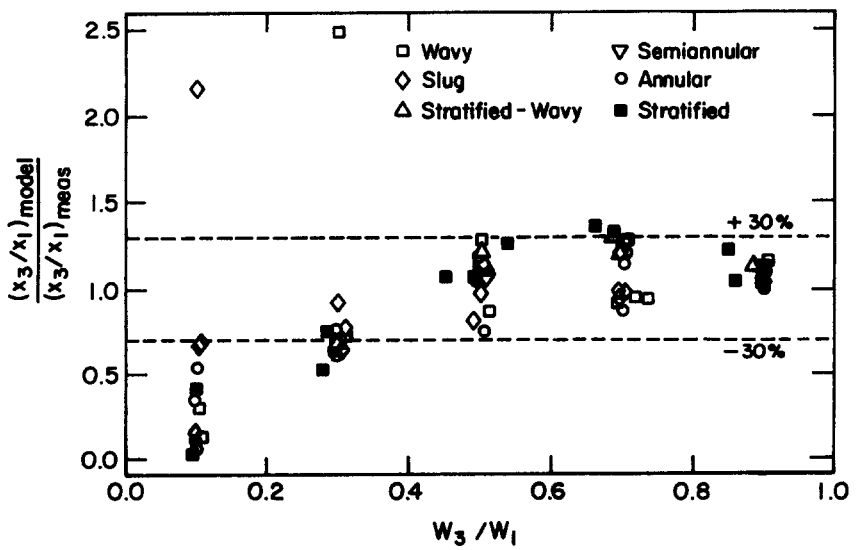

Figure 10. Comparison between the present data and the model of Seeger *et al.* (1986).

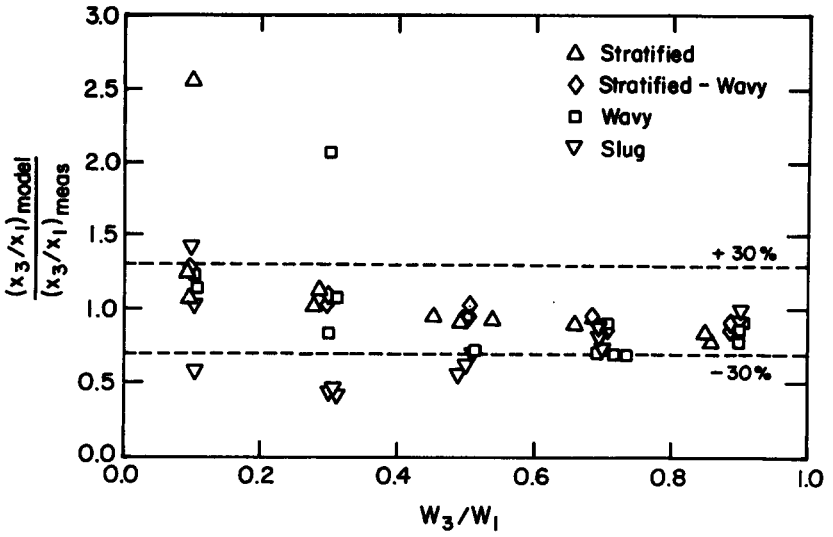

Figure 11. Comparison between the present data of stratified, stratified-wavy, wavy and slug flow and the model of Hwang *et al.* (1988).

3.2. Pressure-drop data

The present data, listed in table 1, provide a fair extension to the previously reported data in terms of liquid velocities, as shown in figures 1 and 5. Different empirical models have been proposed for correlating the previous data with often large disagreements among their predictions. It is highly unlikely that all existing data can be satisfactorily correlated by a single model. Ultimately, a number of flow-regime-specific correlations may be necessary.

No attempt was made in this investigation to develop new models. Rather, it was felt that comparing the present data to the available models in order to assess the models' extendability to the present conditions would be a more useful contribution. Results of these comparisons may guide future developments towards correlations with some form of generalized applicability.

3.2.1. Single-phase flow. For single-phase incompressible flow in a tee junction, a correlation for the inlet-to-run pressure difference is normally derived from a momentum approach as follows:

$$\Delta P_{12} = P_1 - P_2 = K_{12}(G_2^2 - G_1^2)/\rho, \qquad [1]$$

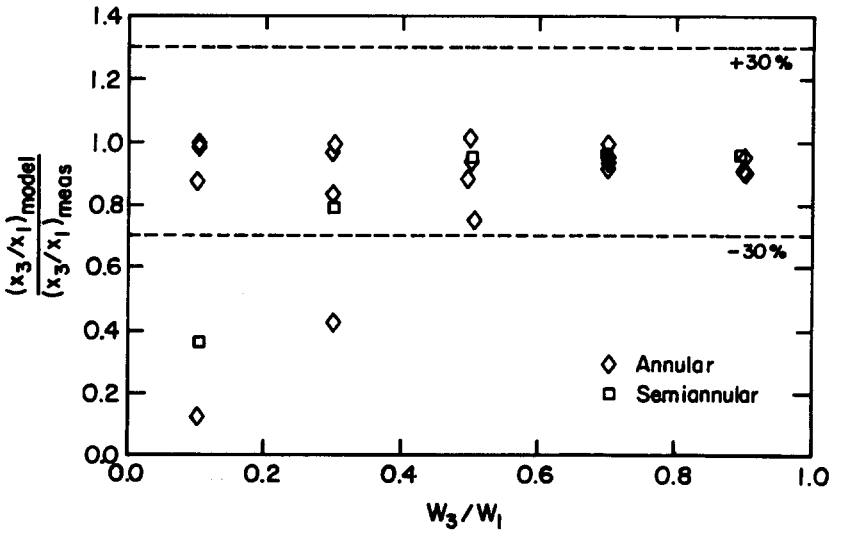

Figure 12. Comparison between the present data of annular and semiannular flow and the model of Hwang *et al.* (1988).

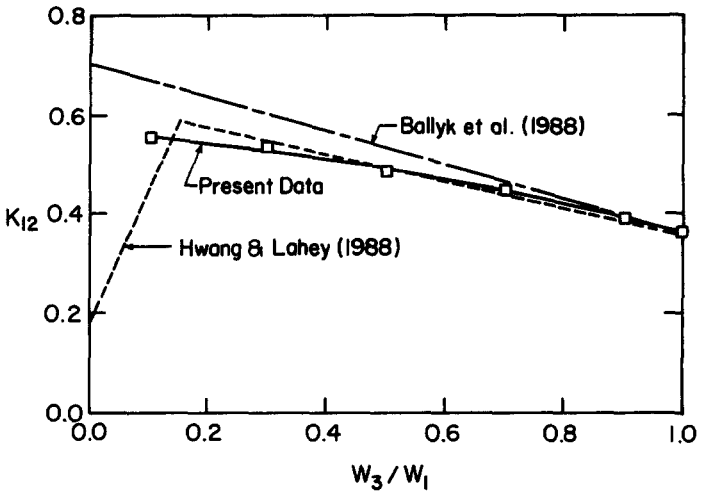

Figure 13. The single-phase momentum correction factor K_{12}.

where P_1 and P_2 are the average pressures at the junction from the inlet and run sides (figure 4), respectively, G_1 and G_2 are the inlet and run mass fluxes, K_{12} is the momentum correction factor and ρ is the density. An energy approach has been frequently adopted for the inlet-to-branch pressure difference, subdividing ΔP_{13} into a reversible component $(\Delta P_{13})_{\text{Rev}}$ and an irreversible component $(\Delta P_{13})_{\text{Irr}}$, thus

$$\Delta P_{13} = P_1 - P_3 = (\Delta P_{13})_{\text{Rev}} + (\Delta P_{13})_{\text{Irr}}, \quad [2]$$

where

$$(\Delta P_{13})_{\text{Rev}} = (G_3^2 - G_1^2)/(2\rho), \quad [3]$$

$$(\Delta P_{13})_{\text{Irr}} = K_{13} G_1^2/(2\rho), \quad [4]$$

P_3 is the average pressure at the junction from the branch side, G_3 is the branch mass flux and K_{13} is a loss coefficient. The energy approach given by [2]–[4] had a fundamental difficulty in correlating ΔP_{12} because it often produces negative values of the loss coefficient for certain conditions, which is physically inconsistent.

Single-phase (liquid) pressure-drop data were obtained in this investigation using seven test runs corresponding to a mean inlet side liquid velocity of 0.18 m/s and $0 \leqslant W_3/W_1 \leqslant 1$. Magnitudes of K_{12} and K_{13} were calculated from the measured values of ΔP_{12} and ΔP_{13} using [1]–[4]. These results are presented in figures 13 and 14, along with other data from previous investigations. Close

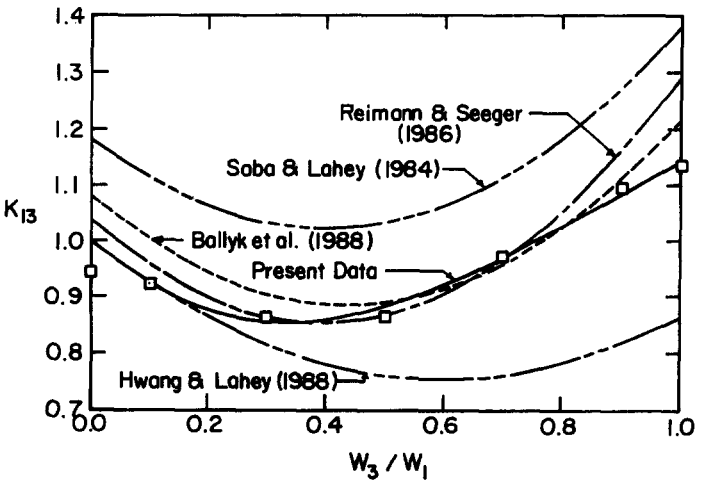

Figure 14. The single-phase loss coefficient K_{13}.

agreement can be seen in figure 13 with Ballyk *et al.* (1988) and Hwang & Lahey (1988) and in figure 14 with Ballyk *et al.* (1988) and Reimann & Seeger (1986). Another comparison was made between the current results and those presented graphically by McNown (1954). This comparison (not shown in figures 13 and 14) produced excellent agreement. In view of the significant differences between the mean inlet velocities used in this investigation and others (e.g. Hwang & Lahey used 1.3–2.6 m/s and Ballyk *et al.* used 0.45–1.2 m/s), it can be concluded from the satisfactory results in figures 13 and 14 that K_{12} and K_{13} are fairly independent of the mass flow rate.

Using the method of least squares, the present data were well correlated by

$$K_{12} = 0.57 - 0.102\eta - 0.107\eta^2, \qquad [5]$$

and

$$K_{13} = 1 - 0.982\eta + 1.843\eta^2 - 0.717\eta^3, \qquad [6]$$

where $\eta = W_3/W_1$ is the extraction rate. Equation [5] does not apply at $\eta = 0$ since K_{12} is not defined at this point. On the other hand, [6] was forced to approach unity at $\eta = 0$ based on physical reasoning.

3.2.2. Two-phase flow. The available correlations for ΔP_{12} and ΔP_{13} during two-phase flow are mostly modifications of the single-phase correlations presented earlier. In general, most of these correlations can be agglomerated into these forms:

$$\Delta P_{12} = K_{12}\left[\frac{G_2^2}{\rho_2} - \frac{G_1^2}{\rho_1}\right], \qquad [7]$$

and

$$\Delta P_{13} = \frac{\rho_{H3}}{2}\left(\frac{G_3^2}{\rho_3^2} - \frac{G_1^2}{\rho_1^2}\right) + K_{13}\frac{G_1^2}{2\rho_L}\phi, \qquad [8]$$

where ρ_1, ρ_2 and ρ_3 are mixture densities in the inlet, run and branch sides, respectively, ρ_{H3} is the homogeneous density in the branch, ϕ is a two-phase loss multiplier and ρ_L is the liquid density.

Predictions from five different models were computed and compared with the present data. The particular specifications of these models are as follows:

(1) Homogeneous flow model (HFM): the two-phase loss multiplier, as suggested by Saba & Lahey (1984), was correlated by $\phi = \rho_L/\rho_{H1}$, correlations [5] and [6] were used for K_{12} and K_{13}, and the homogeneous densities were determined from

$$\rho_{Hi} = \left[\frac{1 - x_i}{\rho_L} + \frac{x_i}{\rho_G}\right]^{-1}, \quad i = 1, 2, 3, \qquad [9]$$

where ρ_G is the gas density and $i = 1$, 2, and 3 for the inlet, run and branch, respectively.

(2) Separated flow model (SFM): correlation [5] was used for K_{12} in [7] and the momentum-weighted densities were used for ρ_1 and ρ_2 in [7], as proposed by Fouda & Rhodes (1974), where

$$\rho_{Mi} = \left[\frac{(1 - x_i)^2}{(1 - \epsilon_i)\rho_L} + \frac{x_i^2}{\epsilon_i\rho_G}\right]^{-1}, \quad i = 1, 2, 3, \qquad [10]$$

ρ_M is the momentum density, and ϵ is the void fraction evaluated from the correlation of Rouhani (1969). In [8] for ΔP_{13}, K_{13} was taken from [6], $\phi = \rho_L/\rho_{M1}$, and the energy-weighted densities were used for ρ_1 and ρ_3, as proposed by Saba & Lahey (1984), where

$$\rho_{Ei} = \left[\frac{(1 - x_i)^3}{(1 - \epsilon_i)^2\rho_L^2} + \frac{x_i^3}{\epsilon_i^2\rho_G^2}\right]^{-0.5}, \quad i = 1, 2, 3, \qquad [11]$$

ρ_E is the energy density and the void fraction ϵ calculated from Rouhani's (1969) correlation.

(3) Hwang & Lahey (1988) model (HLM): in [7], this model employs $\rho_1 = \rho_{M1}$, $\rho_2 = \rho_{H2}$ and K_{12} from [5]. The correlation of Zuber & Findlay (1965) was used in calculating the void fraction, as recommended by Hwang & Lahey. In [8], the HLM specifies $\rho_1 = \rho_{E1}$, $\rho_3 = \rho_{H3}$, $\phi = \rho_L\rho_{H3}/\rho_{H1}^2$ and correlation [6] for K_{13}.

Table 2. Summary of model performances for ΔP_{12}

Model	Interval (%)	% of data predicted correctly: Inlet flow regime: Wavy and stratified-wavy	Slug	Annular and semiannular	Overall
HFM	±50	50	36	83	63
	±30	50	18	79	57
	±20	36	9	46	35
SFM	±50	100	55	100	90
	±30	79	27	88	71
	±20	50	27	79	59
BM	±50	43	73	25	41
	±30	14	64	13	24
	±20	7	55	4	16
RSM	±50	64	36	88	69
	±30	57	27	88	65
	±20	50	27	79	59
HLM	±50	64	73	75	71
	±30	43	64	67	59
	±20	21	55	50	43

(4) Ballyk et al. (1988) model (BM): in [7], this model specifies $\rho_1 = \rho_{M1}$, $\rho_2 = \rho_{M2}$ and $K_{12} = 1$. In [8], the BM specifies $\rho_3 = \rho_{E3}$, an equivalent density for ρ_1 and an empirical formulation for ϕ as a function of the extraction rate.

(5) Reimann & Seeger (1986) model (RSM): for ΔP_{13}, this model uses [8] with $\rho_1 = \rho_{H1}$, $\rho_3 = \rho_{H3}$ and $\phi = \rho_L \rho_{H3} / \rho_{H1}^2$, with [6] for K_{13}. A different method was proposed for ΔP_{12} by splitting it into a reversible pressure difference between the inlet and the throat of a vena contracta in the run and a second pressure difference between the vena contracta and a position downstream in the run.

Table 2 summarizes the performance of the above models against the present ΔP_{12}-data. It is evident that the separated flow model (SFM) gave the best predictions with 71% of the data within ±30% and all the data of wavy, stratified-wavy, semiannular and annular predicted within ±50%. This comparison is shown in figure 15 using $(\Delta P_{21})^{1/3}$ in order to spread out the data. In general,

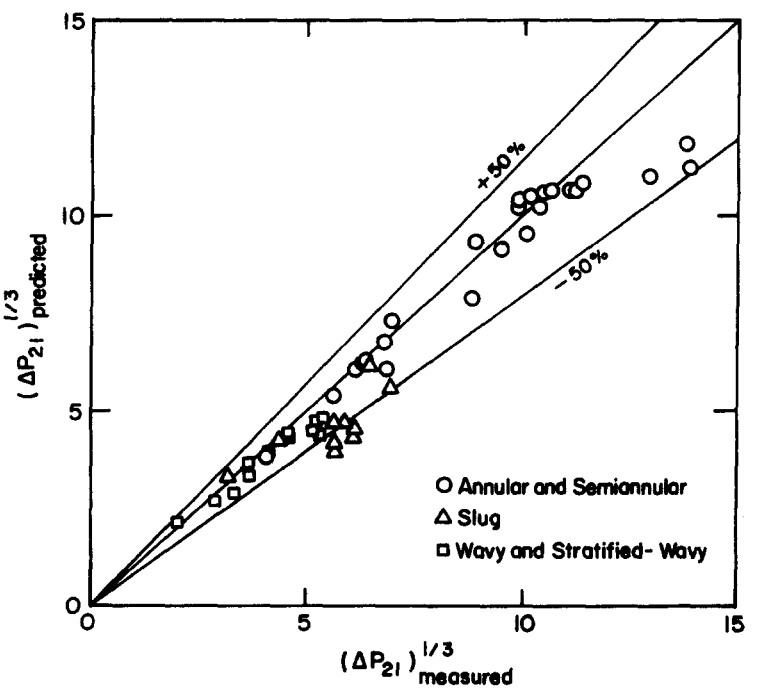

Figure 15. Comparison between the present ΔP_{12}-data and the separated flow model (SFM).

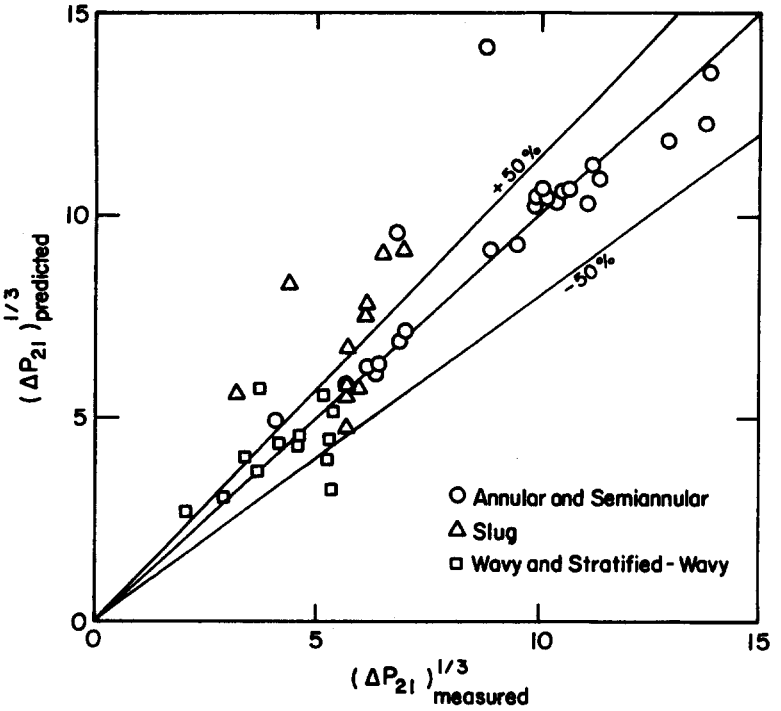

Figure 16. Comparison between the present ΔP_{12}-data and the Reimann & Seeger (1986) model (RSM).

the SFM tended to underpredict the data, more seriously in the slug flow region. The two models that performed best against the slug flow data are BM and HLM. In terms of accuracy of prediction, the second-best model is RSM, shown in figure 16. Again, most of the poor predictions from the RSM are in the slug flow region.

Results of a similar assessment of these models against the ΔP_{13}-data are given in table 3. In general, the performances are less satisfactory than those previously obtained for ΔP_{12}. Interestingly, the SFM and RSM, shown in figures 17 and 18, respectively, are the most accurate models. On closer examination, it can be noted from figure 17 that the SFM had difficulty against data points with $\Delta P_{13} < 0$, which all correspond to $W_3/W_1 \leqslant 0.3$ (according to table 1). On the other hand, the RSM is a better choice in this region according to figure 18. For $W_3/W_1 \geqslant 0.3$, the SFM

Table 3. Summary of model performances for ΔP_{13}

		% of data predicted correctly			
		Inlet flow regime			
Model	Interval (%)	Wavy and stratified-wavy	Slug	Annular and semiannular	Overall
HFM	±50	30	0	59	35
	±30	15	0	55	27
	±20	10	0	41	20
SFM	±50	70	62	68	67
	±30	60	31	41	46
	±20	45	8	27	29
RSM	±50	35	62	73	56
	±30	10	39	64	38
	±20	5	31	41	26
BM	±50	11	39	0	13
	±30	0	15	0	4
	±20	0	8	0	0
HLM	±50	5	0	41	18
	±30	5	0	27	13
	±20	5	0	18	7

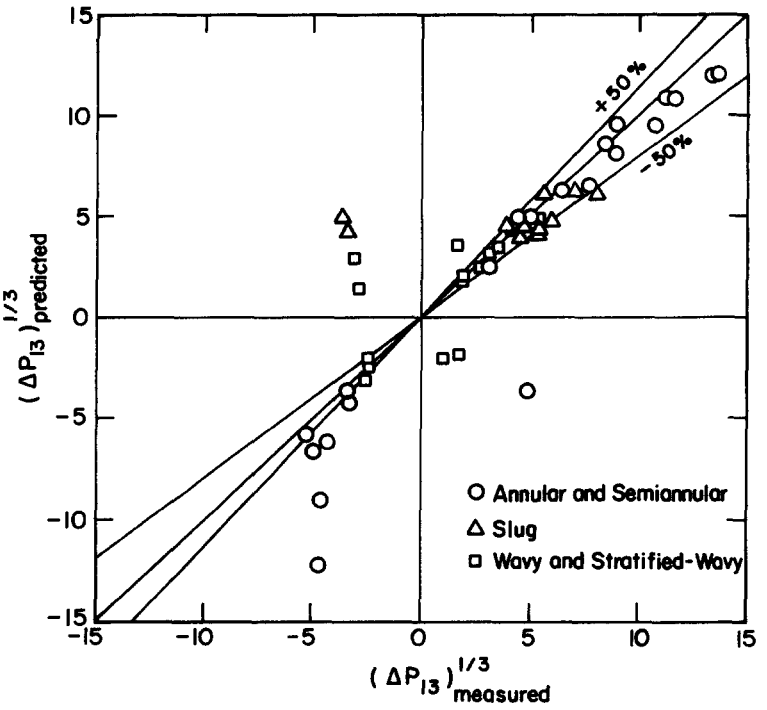

Figure 17. Comparison between the present ΔP_{13}-data and the separated flow model (SFM).

predicts 89% of the data within $\pm 50\%$ and for $W_3/W_1 < 0.3$, the RSM predicts 58% of the data within $\pm 50\%$.

Correlations [5] and [6] obtained in the present study for K_{12} and K_{13}, respectively, were used in the above comparisons. Computations were repeated using the corresponding correlations recommended by various authors. In general, this made little difference to the predictive capability

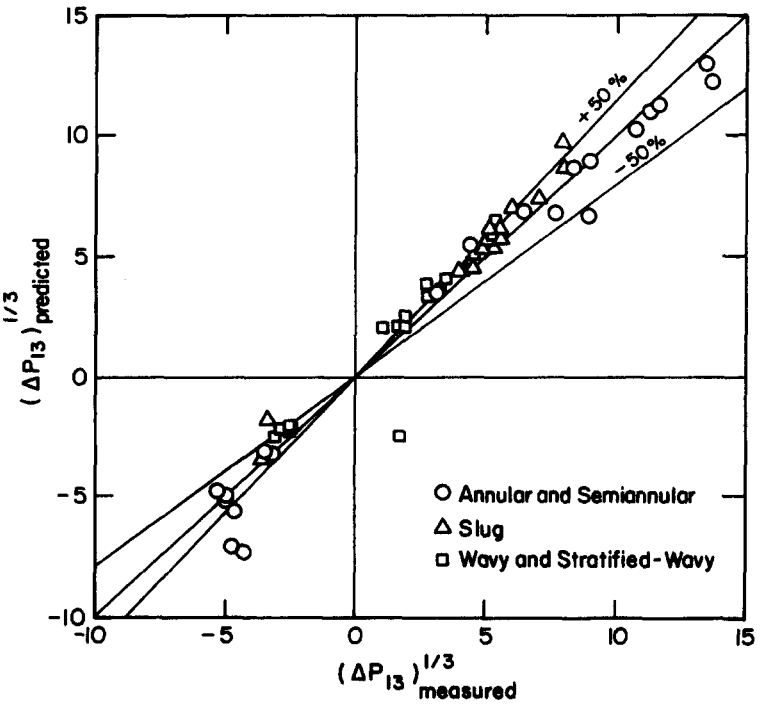

Figure 18. Comparison between the present ΔP_{13}-data and the Reimann & Seeger (1986) model (RSM).

of the models; in fact, the present values of K_{12} and K_{13} usually resulted in slightly better predictions.

It is recognized that all the models used in the above comparisons are empirical and that they were developed from data of significantly higher J_{L1} than the present data. Therefore, while satisfactory agreement may not be expected, the above results could guide the future search for generalized methods of correlating the pressure drops. In this respect, the results shown in figures 15–18 are quite encouraging.

4. CONCLUDING REMARKS

The present experimental investigation provides extensive data for low-pressure, air–water flow in a horizontal, equal-sided tee junction. These data consist of both phase distribution and pressure drops at different extraction rates and a wide range of inlet conditions. The tested range corresponds to inlet flow regimes of stratified, wavy, slug and annular flow with $J_{L1} < 0.2$ m/s. The present pressure-drop data are unique, while the phase-distribution data overlap partially with previous studies.

Similar to previous studies, severe maldistribution of phases generally exists at the junction. The most evident trend displayed by the data is that the preference of the gas to exit through the branch increases as J_{L1} increases at fixed J_{G1}. In general, good agreement in magnitude and trend was obtained in most comparisons with previous data at similar operating conditions. Also, good agreement has been demonstrated against the analytical models of Azzopardi & Whalley (1982) and Hwang *et al.* (1988), and the empirical correlation of Seeger *et al.* (1986) for $W_3/W_1 \geqslant 0.3$.

The pressure differences ΔP_{12} and ΔP_{13} were found to depend on W_3/W_1, J_{G1} and J_{L1}. In general, ΔP_{21} was always positive, while negative values of ΔP_{13} can be obtained with $W_3/W_1 \leqslant 0.3$. Comparisons were made between the present data and five different empirical models developed for significantly higher values of J_{L1}. These comparisons revealed that serious deviations can occur between different models. The best prediction of the present ΔP_{12}-data was produced by a separated flow model, originally proposed by Fouda & Rhodes (1974). In general, less satisfactory predictions were obtained for the ΔP_{13}-data. For $W_3/W_1 \geqslant 0.3$, a separated flow model recommended by Saba & Lahey (1984) gave the best predictions, while for $W_3/W_1 < 0.3$, the model by Reimann & Seeger (1986) gave the best predictions.

Acknowledgement—The financial support provided by the Natural Sciences and Engineering Research Council of Canada is gratefully acknowledged.

REFERENCES

AZZOPARDI, B. J. 1986 Two-phase flow in junctions. In *Encyclopedia of Fluid Mechanics*, Vol. 3, Chap. 25. Gulf Publishing, New York.

AZZOPARDI, B. J. & HERVIEU, E. 1992 Phase separation at T junctions. Presented at the *3rd Int. Workshop on Two-phase Flow*, London, U.K.

AZZOPARDI, B. J. & WHALLEY, P. B. 1982 The effect of flow patterns on two-phase flow in a T junction. *Int. J. Multiphase Flow* **8**, 491–507.

AZZOPARDI. B. J., WAGSTAFF, D., PATRICK, L., MEMORY, S. B. & DOWLING, J. 1988 The split of two-phase flow at a horizontal T: annular and stratified flow. UKAEA Report AERE-R 13059.

BALLYK, J. D. & SHOUKRI, M. 1990 On the development of a model for predicting phase separation phenomena in dividing two-phase flow. *Nucl. Engng Design* **123**, 67–75.

BALLYK, J. D., SHOUKRI, M. & CHAN, A. M. C. 1988 Steam-water annular flow in a horizontal dividing T-junction. *Int. J. Multiphase Flow* **14**, 265–285.

BUELL, J. R. 1992 Two-phase pressure drop and phase distribution in a horizontal tee junction. M.Sc. thesis, University of Manitoba, Winnipeg, Canada.

COLLIER, J. G. 1976 Single-phase and two-phase behaviour in primary circuit components. *Proc. NATO Advanced Study Institute on Two-phase Flow and Heat Transfer*, Istanbul, Turkey.

FOUDA, A. E. & RHODES, E. 1974 Two-phase annular flow stream division in a simple tee. *Trans. Inst. Chem. Engrs* **52**, 354–360.

HART, J., HAMERSMA, P. J. & FORTUIN, J. M. H. 1991 Phase distribution during gas–liquid flow through horizontal dividing junctions. *Nucl. Engng Design* **126,** 293–312.

HENRY, J. A. R. 1981 Dividing annular flow in a horizontal tee. *Int. J. Multiphase Flow* **7,** 343–355.

HONG, K. C. 1978 Two-phase flow splitting at a pipe tee. *J. Petrol. Technol.* **30,** 290–296.

HWANG, S. T. & LAHEY, R. T. 1988 A study on single- and two-phase pressure drop in branching conduits. *Exp. Thermal Fluid Sci.* **1,** 111–125.

HWANG, S. T., SOLIMAN, H. M. & LAHEY, R. T. 1988 Phase separation in dividing two-phase flows. *Int. J. Multiphase Flow* **14,** 439–458.

KATAOKA, I. & ISHII, M. 1983 Entrainment and deposition rates of droplets in annular two-phase flow. *Proc. ASME/JSME Therm. Engng Joint Conf.*, Honolulu, Hawaii, Vol. 1, pp. 69–80.

KLINE, S. J. & MCCLINTOCK, F. A. 1953 Describing the uncertainties in single-sample experiments. *Mech. Engng J.* **75,** 3–8.

LAHEY, R. T. 1986 Current understanding of phase separation mechanisms in branching conduits. *Nucl. Engng Design* **95,** 145–161.

MANDHANE, J. M., GREGORY, G. A. & AZIZ, K. 1974 A flow pattern map for gas-liquid flow in horizontal pipes. *Int. J. Multiphase Flow* **1,** 537–553.

MCNOWN, J. S. 1954 Mechanics of manifold flow. *ASCE Trans.* **119,** 1103–1142.

MULLER, U. & REIMANN, J. 1991 Redistribution of two-phase flow in branching conduits: a survey. Presented at the *Int. Conf. Multiphase Flows*, Tsukuba, Japan.

REIMANN, J. & SEEGER, W. 1986 Two-phase flow in a T-junction with a horizontal inlet—Part II: pressure differences. *Int. J. Multiphase Flow* **12,** 587–608.

REIMANN, J., BRINKMANN, H. J. & DOMANSKI, R. 1988 Gas–liquid flow in dividing tee-junctions with a horizontal inlet and different branch orientations and diameters. Kernforschungszentrum Karlsruhe, Report KfK 4399.

ROUHANI, Z. 1969 Modified correlations for void and two-phase pressure drop. AB Atomenergi Sweden, Report AE-RTV-841.

RUBEL, M. T., SOLIMAN, H. M. & SIMS, G. E. 1988 Phase distribution during steam–water flow in a horizontal tee junction. *Int. J. Multiphase Flow* **14,** 425–438.

SABA, N. & LAHEY, R. T. 1984 The analysis of phase separation phenomena in branching conduits. *Int. J. Multiphase Flow* **10,** 1–20.

SEEGER W., REIMANN, J. & MULLER, U. 1986 Two-phase flow in a T-junction with a horizontal inlet—Part I: phase separation. *Int. J. Multiphase Flow* **12,** 575–585.

SHOHAM O., BRILL, J. P. & TAITEL, Y. 1987 Two-phase flow splitting in a tee junction: experiment and modeling. *Chem. Engng Sci.* **42,** 2667–2676.

TSUYAMA, M. & TAGA, M. 1959 On the flow of the air–water mixture in the branch pipe—1. Experiment on the horizontal branch which is equal to the main one in diameter. *Bull. JSME* **2,** 151–156.

WALPOLE, R. E. & MYERS, R. H. 1985 *Probability and Statistics for Engineers and Scientists*, 3rd edn. Macmillan, New York.

WHALLEY, P. B. & AZZOPARDI, B. J. 1980 Two-phase flow in a T junction. UKAEA Report AERE-R 9699.

ZUBER, N. & FINDLAY, J. A. 1965 Average volumetric concentration in two-phase flow systems. *J. Heat Transfer* **87,** 453–458.